Hindawi
Advances in Materials Science and Engineering
Volume 2019, Article ID 4752478, 11 pages
https://doi.org/10.1155/2019/4752478

Research Article

Recommendation of Suitable Loading Waveforms and Wavelength Equations for Dynamic Modulus Based on Measured Wheel Loads

Xiongwei Dai[1], **Xiaodi Hu**[2] **and Ying Gao**[1]

[1]*School of Transportation, Southeast University, Nanjing 210096, China*
[2]*Transportation Research Center, Wuhan Institute of Technology, Wuhan 430073, China*

Correspondence should be addressed to Xiongwei Dai; daixiong.wei@163.com

Received 14 May 2019; Accepted 15 July 2019; Published 28 July 2019

Academic Editor: Victor M. Castaño

Dynamic modulus is a key parameter in the pavement structure design and analysis. A haversine loading waveform is the most widely recommended waveform in the laboratory to obtain the dynamic modulus of asphalt mixtures by test protocols, which may not completely represent all field loading conditions. The aim of this study is to investigate the suitable vertical compressive stress pulse waveforms at different depths under different pavement structures and to obtain the best fitting waveforms by using the least squares method. Specifically, the vertical compressive stress of different pavement structures was calculated by utilizing a three-dimensional finite element program incorporating with the measured wheel loads. The results revealed that the vertical stress pulse waveforms at different depths in asphalt layer were different within different pavement structure combinations. Generally, the square waveform fitted the vertical stress pulse waveform better for the shallow depth of the surface layer. The haversine waveform became more suitable while the depth increased. The bell waveform was better when the depth went deeper (i.e., 10 cm). In addition, the method of choosing waveforms at different depths of different pavement structures was provided, and the equation of calculating wavelength was recommended. Moreover, dynamic modulus under different loading waveforms were analysed through laboratory test, and the process for obtaining dynamic modulus of asphalt layer in any depth was presented.

1. Introduction

The mechanistic-empirical (M-E) is one of the fundamental methods that is routinely used for the asphalt pavement structural design and analysis. The most recent and successful achievement in the application and further enhancement of the M-E method is the development of the Mechanistic-Empirical Pavement Design Guide (M-EPDG) [1]. The dynamic modulus is one of the basic parameters as the input material property [1]. In laboratory, the dynamic modulus value of the hot mixture asphalt (HMA) is typically determined as a function of the test temperature, loading waveform, and frequency [2].

A haversine waveform is utilized as the loading waveform to obtain dynamic modulus corresponding to laboratory test methods [3–7]. In reality, the vertical compressive stress varies along with the pavement depth, which leads to the waveform of the vertical compressive stress pulse also vary at different depths within the asphalt concrete (AC) layer. The haversine loading waveform may not fully be simulative for the field loading conditions [8]. Based on the research result of Barksadale, the vertical compressive stress pulse could be fitted by the haversine waveform at pavement surface position [9]. Furthermore, according to the literature [10], the vertical compressive stress pulse waveform tended to approach a square waveform while the point of interest was close to the surface of the pavement and changed to a haversine as the depth increases. The shape of the vertical compressive stress pulse waveform approached a triangular one at deeper position in the AC layer. Moreover, haversine and bell waveforms could fit the vertical compressive stress pulse waveforms well for a moving vehicle [11].

Loading frequency can be calculated by loading time. Previous research has shown that loading time is closely

related to the wavelength of vertical compressive stress, depth of interest, and vehicle speed. Hu et al. introduced an iterated method to calculate the loading time [10]. Brown derived an equation to calculate the loading time, and the relationship between loading time, t (s), depth, d (m), and vehicle speed, v (km/h), was defined as follows [12]:

$$\log(t) = 0.5\,d - 0.2 - 0.94\log(v). \quad (1)$$

Huang proposed a haversine waveform to fit moving load in the VESYS and Kenlayer program, and loading time (d_i) was calculated as follows [13]:

$$d_i = \frac{12a_i}{s}, \quad (2)$$

where a_i is the tire contact radius for each axle type and s is the vehicle speed.

Several study results have shown that the tire contact area is not a simple circular shape, and the vertical tire-pavement contact pressure (TPCP) is not uniformly distributed [14–17]. The measured TPCP is nonuniformly distributed and changes with the discrepancy in axle load, tire inflation pressure, tire type, and tire tread patterns [15]. As a result, the mechanical responses are inaccurate if a circular uniformly distributed load is considered, which significantly affects the vertical compressive stress in the pavement structure. Therefore, the measured TPCP can be used to calculate more accurate vertical compressive stress and obtain an accurate vertical compressive stress pulse waveform. Furthermore, it provides an accurate loading waveform on obtaining dynamic modulus in the laboratory test and precise parameters for pavement structure design.

This study focuses on calculating the vertical compressive stress by using the measured wheel loads and then obtaining waveforms of the vertical compressive stress pulse. A three-dimensional finite element (3D-FE) program incorporated with the measured vertical TPCP and horizontal forces (i.e., lateral pressure) is utilized to calculate the vertical compressive stress. The objectives are to investigate the accurate loading waveforms, wavelength, and loading time at different depths in the AC layer under different combinations of layer thickness and AC modulus. Besides, this study demonstrates the method to acquire precisely dynamic modulus at different depths for the field AC layer through the laboratory test.

2. Methodology

2.1. 3D-FE Model. For mechanistic response analyses, it is more reasonable to adopt nonlinear viscoplastic models to fit the field pavement conditions [18–20]. However, it is proved that using multilayer linear elastic theory for modelling the AC layer, base layer, and subgrade is satisfactorily verified with measured field data [10, 21]. In addition, it is less time-consuming. Therefore, the 3D-FE multilayer linear elastic model was chosen in this study.

Figure 1 illustrates the 3D-FE model for analysis. The dimension of this model was 5 m × 10 m × 6 m. The boundary conditions were assumed to be as follows: (1) zero Z-directional displacement at the bottom, (2) zero X-directional displacement on both sides, and (3) zero Y-directional displacement on both sides. As previously mentioned, the aim of this study was to investigate the vertical compressive stress under the measured vertical TPCP and horizontal forces; thus, only the maximum vertical compressive stress within the pavement structure was modelled and analysed in the following part.

2.2. Loading Parameters. According to the literature [15], the longitudinal tread pattern tire is one of the most common types of tires in China, which was chosen for TPCP modelling. Moreover, 3D loads (vertical and horizontal loads) were used to represent the tire-pavement pressure of the moving load under a constant speed in this study. The obtained moving load was uniformly distributed on the node of each meshed unit in the 3D-FE model. The simplified 3D-FE model for tire-pavement contact area and the loading pattern on the 3D-FE model were illustrated, as shown in Figure 2. As shown in Figure 2(c). It should be noted that the vertical and horizontal TPCP directions acting on the nodes of each rib is completely symmetrical. Total weight of the rear axle of 100 kN, tire pressure of 600 kPa, and a single wheel load of 25 kN were implemented to the model. The measured vertical TPCP was consistent with the tire tread pattern, which was used to compute the vertical and horizontal stress [15]. Based on the available literature, the lateral tire contact stress was generally in the perpendicular direction and approximately 15% to 50% of the maximum vertical compressive stress [22–25]. Besides, lateral tire contact stress was taken as 30% of the maximum vertical compressive stress. The longitudinal stress was considered to be 12% of the maximum vertical compressive stress [25].

2.3. Pavement Structure. Typical AC layer thickness, namely, 2.5 cm, 3.8 cm, 5 cm, 7.5 cm, 10 cm, 15 cm, 20 cm, and 30 cm, was investigated. The thickness of two base layers was 20 cm. The literature [10] showed that the modulus ratio (R) between the layer of interest and the immediate succeeding layer below has a significant influence on the vertical compressive stress waveform. R values were considered as 0.02, 0.05, 0.5, 1, 5, 20, and 50 in this study. It should be noted that when calculating the vertical stress, the thickness equivalent conversion of the multilayer asphalt pavement structure was still valid [9, 10]. On this basis, in order to simplify the model, only one layer of AC was selected. The minimum and maximum moduli of the AC layer are 1,000 MPa and 10,000 MPa, respectively. The moduli of two base layers were set the same, and the value was between 10 MPa and 200,000 MPa. Similarly, the moduli of subgrade were between 10 MPa and 1,000 MPa. The modulus and thickness of various pavements were considered which covered most of the commonly used pavement structures. More than 1,000 cases were analysed in the study.

3. Analysis of Vertical Compressive Stress Pulse Waveform

The vertical compressive stress pulse is different at various depths, and three shapes of waveforms were utilized to fit the

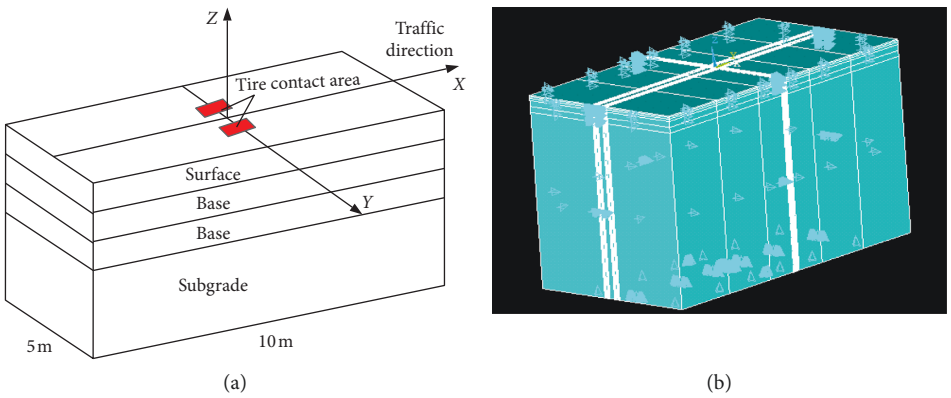

Figure 1: The 3D-FE model: (a) dimension; (b) boundary conditions.

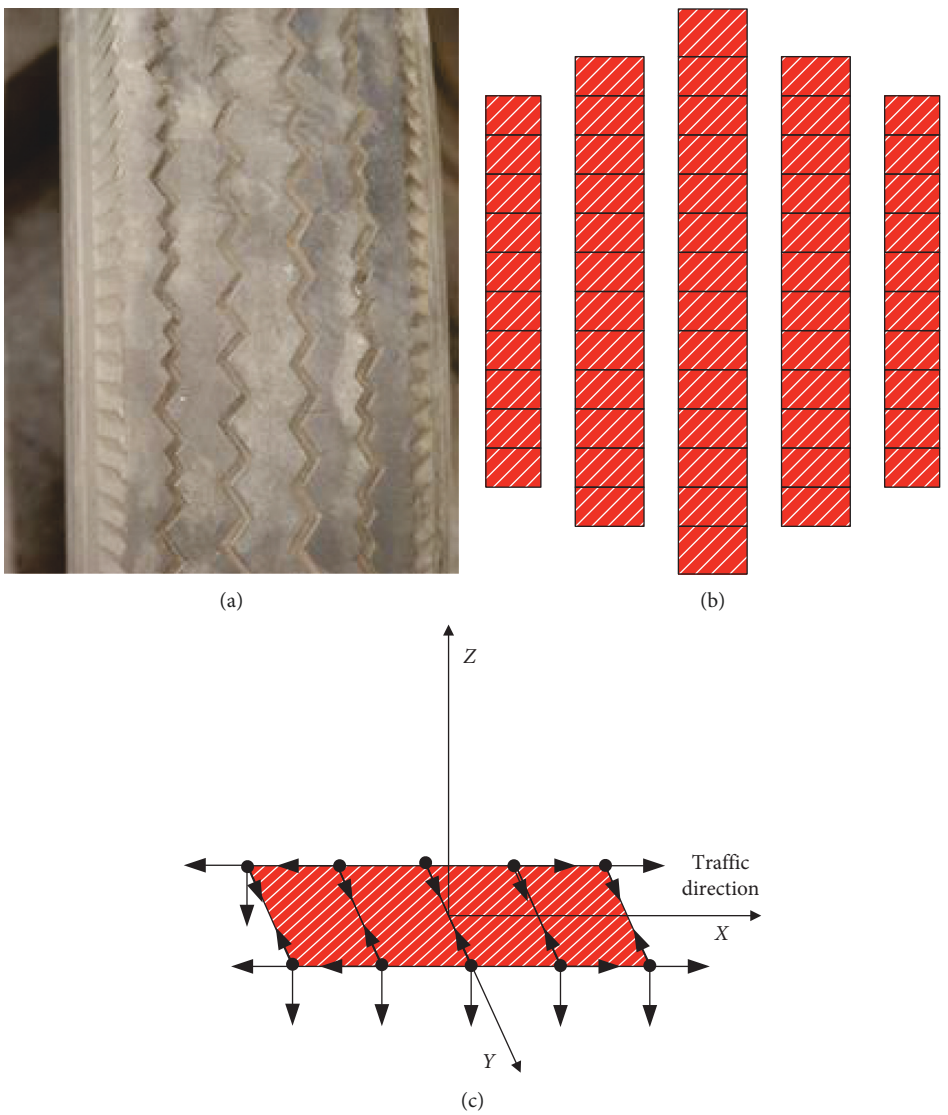

Figure 2: Tire-pavement contact area: (a) longitudinal tread pattern tire; (b) simplified tire-pavement contact area for the 3D-FE model; (c) vertical and horizontal TPCP directions acting on the nodes of part mesh units.

curves. Moreover, the least squares method was used to choose the optimal fitting waveform.

3.1. Equations for Fitting the Vertical Compressive Stress. Researchers utilized square, haversine, triangle, and bell waveforms to fit the vertical compressive stress pulse waveform of the AC layer. The results demonstrated that the vertical compressive stress pulse waveform changed at different depths in the AC layer [8–11]. In addition, according to the analysis results, the triangle waveform could not fit the vertical compressive stress pulse waveform appropriately. However, square, haversine, and bell waveforms could fit the vertical compressive stress pulse waveform at different depths in different pavement structures. As a result, square, haversine, and bell waveforms were selected. Fitting equations for the square, haversine, and bell waveforms are listed in the following equations, respectively:

$$\text{square waveform shape: } y = 1\left(x \le \frac{d}{2}\right), \tag{3}$$

$$\text{haversine waveform shape: } y = \sin^2\left(\frac{\pi}{2} + \pi * \frac{x}{d}\right), \tag{4}$$

$$\text{bell waveform shape: } y = \frac{1}{e^{-(x/d)^2}}, \tag{5}$$

where d (m) is the length of the vertical compressive stress pulse and x (m) is the horizontal distance between the point of interest and the centre of the loading.

3.2. Process of Choosing the Best Fitting Waveform. As previously stated, three different waveforms were utilized to fit the vertical compressive stress pulse waveforms. The method of normalizing the vertical compressive stress was beneficial for obtaining suitable fitting curves. The steps for selecting the best fitting waveform curves were as follows:

(1) The vertical compressive stress was calculated by the 3D-FE model at each depth. The maximum vertical compressive stress distribution along the traffic direction was selected as the representative for analysis.

(2) The normalized vertical compressive stress pulse waveform was calculated by the ratio of vertical compressive stress value to its maximum value along the traffic direction at the same depth.

(3) The normalized vertical compressive stress pulse waveform were fitted by using equations (3)–(5), respectively.

(4) The optimal curve was chosen by the least squares method.

3.3. Vertical Compressive Stress Pulse Waveform in the Same Pavement Structure. Due to the length of the article, in this part and the following part, only parts of the fitting results were demonstrated.

S-Z indicates the normalized vertical compressive stress pulse waveform. S and D indicate the wavelength of the square waveform, and the best fitting waveform at the given depth was the square waveform. H and D represent the wavelength of the haversine waveform, and the best fitting waveform at the given depth was the haversine waveform. B and D indicate the wavelength of the bell waveform, and the best fitting waveform at the given depth was the bell waveform. Z (cm) is the vertical depth between the point of interest and the pavement surface.

The vertical compressive stress at different depths in the AC layer was calculated, and the pavement structure was as follows: the thickness of the AC layer was 20 cm, and the moduli of AC layer, base, and subgrade were 1,000 MPa, 20,000 MPa, and 50 MPa, respectively. The fitting results were at the depths of 0 cm, 5 cm, 10 cm, and 17.8 cm, as shown in Figure 3.

(1) The vertical compressive stress pulse varied with the depth of interest changed. Meanwhile, the length of the vertical compressive stress pulse increased as the depth increased. Optimal fitting waveform for the vertical compressive stress was not always haversine. As the depth of interest increased, the optimal fitting waveform was square at shallow position, in Figure 3(a). Then, it changed to haversine, in Figure 3(b). On a comparison basis, the bell waveform was the best fitting shape curve at deeper position ($Z = 17.8$ cm), in Figure 3(d). In conclusion, the depth was a main factor influencing the shape and wavelength of vertical compressive stress pulse.

(2) Two waveforms could be used to fit and define the vertical compressive stress at a particular depth, in Figure 3(c). Both the haversine and bell waveforms could be utilized to fit the vertical compressive stress waveforms at $Z = 10$ cm; additionally, the wavelengths of the two kinds of waveforms were close.

3.4. Vertical Compressive Stress Pulse Waveform in Different Pavement Structures. Four groups of modulus combinations of the surface AC layer, base, and subgrade were selected for this analysis at two different depths. R values of four pavement structures were 0.5, 0.5, 1, and 20, respectively. The fitting results of vertical compressive stress pulse are shown in Figure 4. In the figure, the following can be observed:

Figure 4(a): the thickness of the AC layer was 15 cm, moduli of the pavement structure were 1,000 MPa, 2,000 MPa, and 40 MPa for the AC layer, base layer, and subgrade, respectively, and the position of interest was at a depth of 10 cm.

Figure 4(b): the thickness of the AC layer was 15 cm, moduli of the pavement structure were 10,000 MPa, 20,000 MPa, and 100 MPa for the AC layer, base layer, and subgrade, respectively, and the position of interest was at a depth of 10 cm.

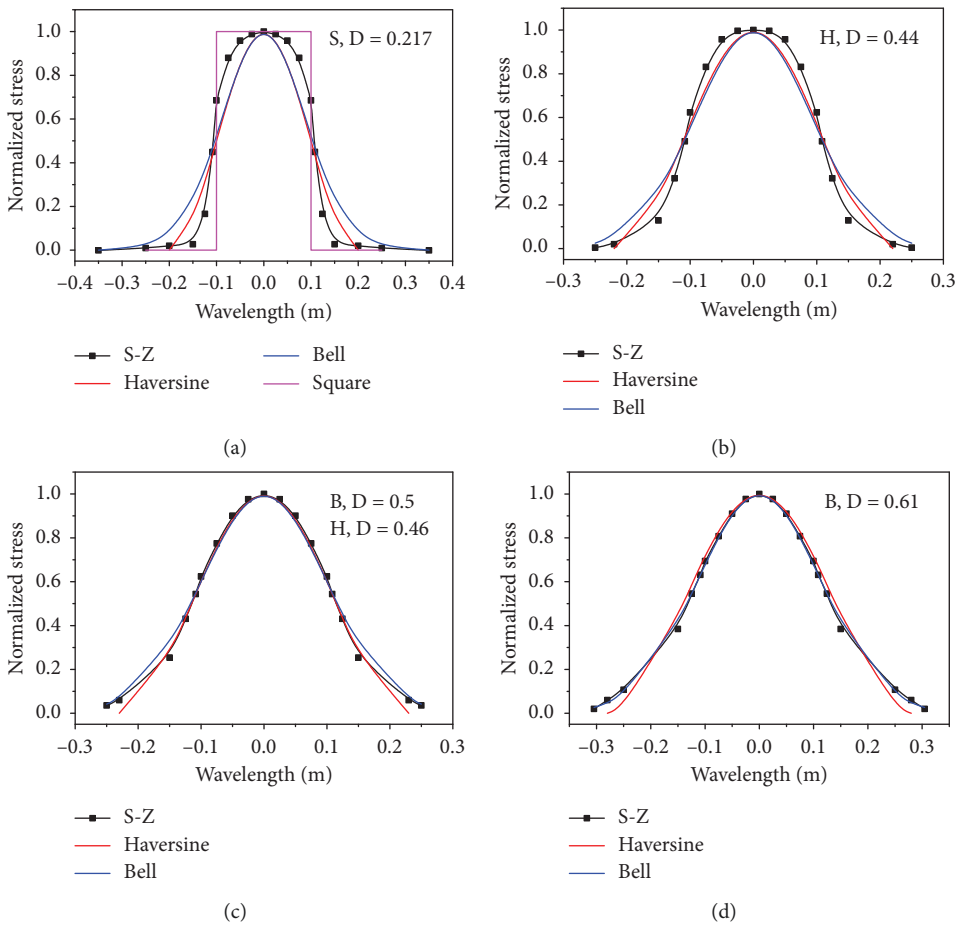

Figure 3: Vertical compressive stress pulse at different depths in the same pavement structure: (a) $Z = 0$ cm, (b) $Z = 5$ cm, (c) $Z = 10$ cm, and (d) $Z = 17.8$ cm.

Figure 4(c): the thickness of the AC layer was 30 cm, moduli of the pavement structure were 1,000 MPa, 1,000 MPa, and 30 MPa for the AC layer, base layer, and subgrade, respectively, and the position of interest was at a depth of 20 cm.

Figure 4(d): the thickness of the AC layer was 30 cm, moduli of the pavement structure were 10,000 MPa, 500 MPa, and 20 MPa for the AC layer, base layer, and subgrade, respectively, and the position of interest was at a depth of 20 cm.

In Figure 4, the following conclusions could be drawn:

(1) Comparing Figures 4(a), 4(c), and 4(d) and Figures 4(b), 4(c), and 4(d), the vertical compressive stress pulse waveform changed with different R values, thickness of pavement structures, and different depths; additionally, wavelength was not the same.

(2) In Figures 4(a) and 4(b), among different pavement structures, when the R value and the thickness of AC layer were the same, regardless of the modulus of AC value, the vertical compressive stress pulse waveform was the same. Moreover, haversine and bell waveforms could fit the vertical compressive stress pulse waveform well at a certain depth, and the wavelength of two waveforms was close. The R value was one of the key factors that affect the waveform and wavelength, and the modulus of subgrade had a little effect on waveform and wavelength.

(3) In Figures 4(c) and 4(d), the bell waveform fitted the vertical compressive stress pulse waveform well in deeper position of pavement structure, i.e., at a depth of 20 cm. Wavelength increased with the increase in the R value within the same thickness of the pavement structure.

4. Recommended Waveforms and Wavelength for Each Depth

Numerous computations and analyses were conducted in this study. Based on these analyses, the appropriate loading waveform and wavelength were proposed for different depths in the AC layer. The depth of interest and the R value were the two main factors that affected the waveforms and wavelength. The following part stated the method to obtain appropriate loading waveform and wavelength at any depth in the AC layer.

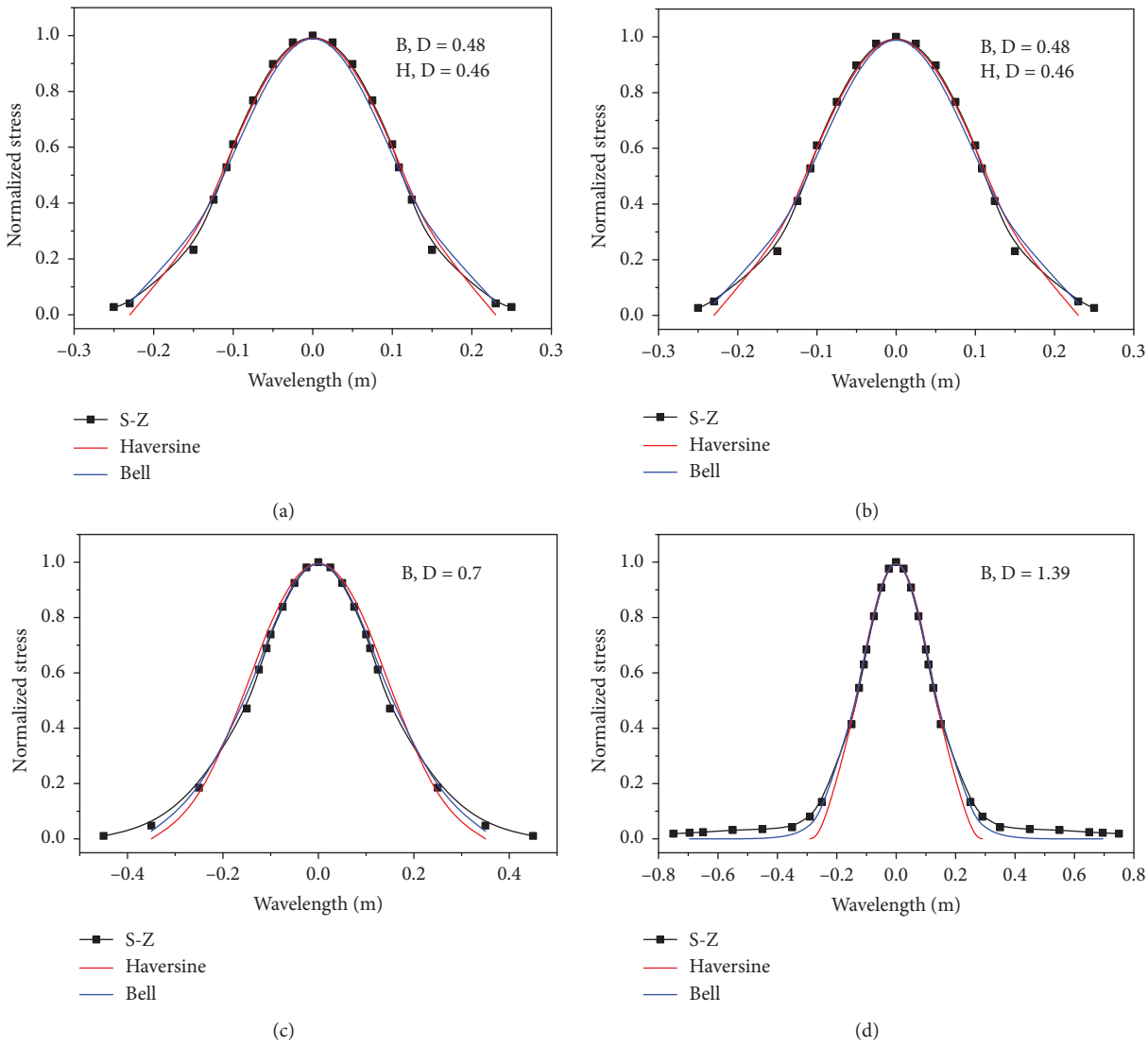

Figure 4: Vertical compressive stress pulse with different pavement structures: (a) $R = 0.5$, $Z = 10$ cm; (b) $R = 0.5$, $Z = 10$ cm; (c) $R = 1$, $Z = 20$ cm; (d) $R = 20$, $Z = 20$ cm.

H_{AC} (cm) represented the thickness of the AC layer, h (cm) represented the depth of the position of interest, the R value was the modulus ratio between the layer of interest and the immediate succeeding layer below, and D (cm) was the wavelength of the vertical compressive stress pulse.

5. Recommended Proper Waveform for Each Depth

According to more than 1,000 cases of computation and analyse results, appropriate loading waveform was suggested. The following steps were the methods to get a proper waveform at different depths in different pavement structures:

(1) A square waveform was suggested for a pavement depth within the range $0 < h < 2.5$ cm, regardless of the AC layer thickness.

(2) A haversine waveform was recommended for a pavement depth range of $2.5\text{ cm} \le h < 5$ cm when $2.5\text{ cm} \le H_{AC} < 5$ cm.

(3) A haversine waveform was proposed when $5\text{ cm} \le H_{AC} \le 10$ cm and for a pavement depth range of $2.5\text{ cm} \le h < 0.5\ H_{AC}$. Furthermore, for $0.5H_{AC} \le h \le H_{AC}$ and $0.02 \le R \le 5$, a haversine waveform was proposed, and bell waveform was applicable for the other cases.

(4) A haversine waveform was found to be appropriate when $10\text{ cm} < H_{AC}$, at a position of $2.5\text{ cm} \le h \le 5$ cm. For the other case scenarios, the following steps were used to select the appropriate loading waveform:

(4.1) A haversine waveform was recommended when $10\text{ cm} < H_{AC} < 20$ cm. $5\text{ cm} < h \le 7.5$ cm. Moreover, when $h > 7.5$ cm, both the haversine and bell waveforms could satisfactorily fit the

vertical stress pulse when $R \leq 1$. However, when $R > 1$, the bell waveform exhibited better curve fitting tendency than the haversine waveform.

(4.2) A haversine waveform was recommended when $20\,\text{cm} \leq H_{AC}$ and $5\,\text{cm} < h \leq 10\,\text{cm}$. For other depths, the bell waveform was more suitable.

5.1. Recommended Wavelength for Each Depth. Depending on the optimal fitting waveforms that were recommended at different depths, simultaneously, wavelength could be obtained. The wavelength could be divided into four conditions for analysis, namely, (1) condition 1: $0 < h < 2.5\,\text{cm}$; (2) condition 2: $2.5\,\text{cm} \leq H_{AC} \leq 3.8\,\text{cm}$; (3) condition 3: $3.8\,\text{cm} < H_{AC}$ and $h \leq 0.5757 H_{AC} + 0.0424$; and (4) condition 4: else. The fitting equations of wavelength for each condition were proposed, as presented in Table 1. The wavelength was mainly affected by the depth of interest in the shallow position (i.e., 3.8 cm) based on the equations of wavelength.

The wavelength was 21.7 cm for condition 1, equal to the maximum length of the tire tread. Figure 5(a) illustrates the wavelength under conditions 2 and 3, and the wavelengths could be fitted accurately by equations (*) and (**), respectively. As presented in Figures 5(b) and 5(c), the wavelength corresponds to different R and h. Besides, equation (***) fitted the wavelength of condition 4 properly.

6. Dynamic Modulus of Different AC Layers

The dynamic modulus of AC at various temperatures and frequencies could easily be obtained under different loading waveforms by the laboratory test [2]. In this section, the method and example of obtaining dynamic modulus for random depth of the AC layer was presented.

6.1. Method for Obtaining Dynamic Modulus. Figure 6 illustrates a typical pavement structure. The AC layer was divided into several sub-AC layers, the thickness was h_{ACi}, the modulus was $E_{Sub\text{-}ACi}$, and the depth of interest was h_i.

The modulus was calculated from the lower position to the upper position. The iteration method was used to obtain the loading waveforms, wavelength, frequency, and dynamic modulus. The difference between two calculated modulus values was less than 1%, which meant the modulus was appropriate. The method of obtaining dynamic modulus depends on the waveform and wavelength, as shown in Figure 7.

Loading time (T) could easily be calculated by using equation (6). Loading frequency (f) could be expressed by using equation (7):

$$T = \frac{D}{v}, \tag{6}$$

$$f = \frac{1}{T}, \tag{7}$$

where D is the wavelength and v is the vehicle speed.

In addition, dynamic modulus curves under different loading waveforms at a certain temperature could be fitted by using the following equation:

$$E_{AC} = E(f). \tag{8}$$

6.2. Example of Obtaining Dynamic Modulus. The common pavement structure in China and the probable loading waveform for each layer are presented in Table 2.

All the test samples of AC-13/20/25 were molded a target air void of $4 \pm 1\%$, as specified by "Technical specification for construction of highway asphalt pavements" [26]. As shown in Figure 8, the dynamic moduli of AC-13, AC-20, and AC-25 under different loading waveforms at the temperature of 21°C were obtained. The dynamic modulus curves under different loading waveforms were different. Within the same test condition, dynamic modulus values under the square loading waveform were much smaller than those under haversine and bell loading waveforms. Each E^* curve was fitted as presented in equations (9)~(14) (E^* is the dynamic modulus, and f is the loading frequency):

$$\text{AC-25-haversine: } E^* = 2531 \ln(f) + 8003, \quad R^2 = 0.97, \tag{9}$$

$$\text{AC-20-haversine: } E^* = 2380 \ln(f) + 6868, \quad R^2 = 0.97, \tag{10}$$

$$\text{AC-13-haversine: } E^* = 2332 \ln(f) + 5872, \quad R^2 = 0.95, \tag{11}$$

$$\text{AC-25-bell: } E^* = 1986 \ln(f) + 7042, \quad R^2 = 0.99, \tag{12}$$

$$\text{AC-20-bell: } E^* = 1919 \ln(f) + 5813, \quad R^2 = 0.98, \tag{13}$$

$$\text{AC-13-square: } E^* = 335.9 \ln(f) + 1209, \quad R^2 = 0.95. \tag{14}$$

The pavement structure has, as shown in Table 2, $H_{AC} = 18\,\text{cm}$. According to "Specifications for design of highway asphalt pavements" [27], the modulus of the base layer: $E_B = 18{,}000\,\text{MPa}$ and the modulus of the subgrade: $E_s = 50\,\text{MPa}$. In general, considering the minimum speed of China's high-grade highway is 60 km/h, the speed was set as 72 km/h = 20 m/s.

Based on the methodology of obtaining dynamic modulus for the depth of interest as presented in Figure 7, the dynamic modulus, wavelength, frequency, and loading waveforms at the depth of $h_1 = 2\,\text{cm}$, $h_2 = 7\,\text{cm}$, and $h_3 = 14\,\text{cm}$ were calculated as follows:

(1) $h_3 = 14\,\text{cm}$. The modulus at a depth of 14 cm was assumed as $E_3 = 20{,}000\,\text{MPa}$.

Table 1: Wavelength at different depths.

Depth condition	Wavelength/cm	Correlation coefficient
$0 < h < 2.5$ cm	$D = 21.7$	N/A
$2.5\text{ cm} \le H_{AC} \le 3.8$ cm	$D = -21.018h^2 + 151.73h - 227.75$ (*)	0.987
$3.8\text{ cm} < H_{AC}$, and $h \le 0.5757H_{AC} + 0.0424$	$D = 2.205h + 32.55$ (**)	0.980
Else	$D = 30.38 + 0.1469 * R + 1.829 * h - 0.04423 * R^2 + 0.3268 * R * h + 0.0008164 * R^3 - 0.004176 * R^2 * h$ (***)	0.987

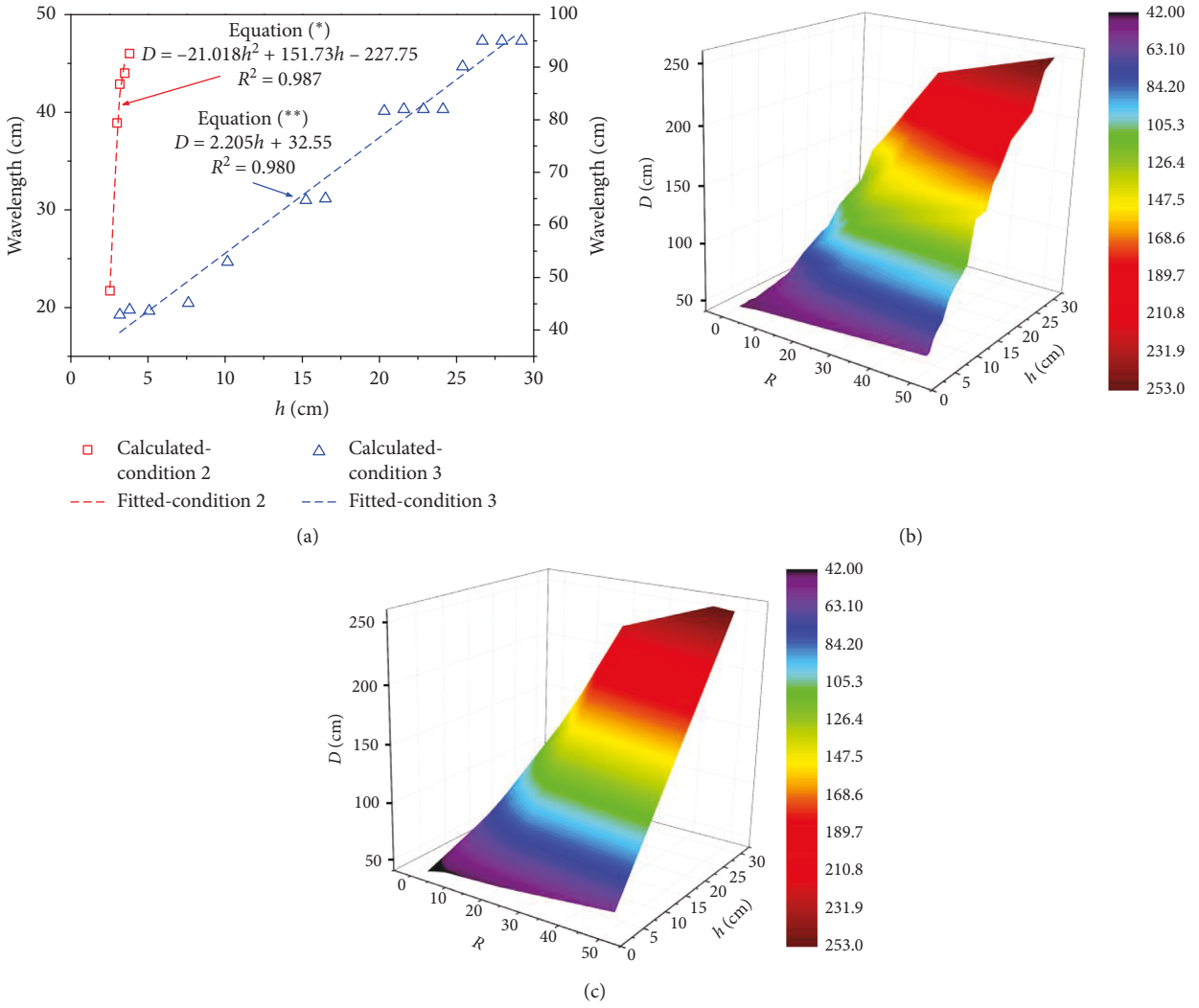

Figure 5: Wavelength under different combinations of R and h: (a) wavelength for equations (*) and (**); (b) calculated wavelength for equation (***); (c) fitted wavelength by using equation (***).

$1 < R_3 = E_3/E_B$. Loading waveform: bell waveform. Via equation (***), wavelength: $D_3 = 61.870$ cm, loading time: $T_3 = 0.0309$ s, and loading frequency: $f_3 = 32.326$ Hz. Via equation (12), $E_{3\text{-}1} = 13{,}945$ MPa.

$R_{3\text{-}1} = E_{3\text{-}1}/E_B < 1$. Loading waveform: haversine and bell waveforms. Via equation (***), wavelength: $D_{3\text{-}1} = 60.138$ cm, loading time: $T_{3\text{-}1} = 0.0301$ s, and loading frequency: $f_{3\text{-}1} = 33.257$ Hz.

(1.1) Loading waveform: bell waveform. Via equation (12), $E_{3\text{-}1\text{-}1} = 14{,}001$ MPa.
Then, $|E_{3\text{-}1\text{-}1}\text{-}E_{3\text{-}1}|/E_{3\text{-}1} \le 1\%$; therefore, $E_3 = E_{3\text{-}1\text{-}1} = 14{,}001$ MPa.

(1.2) Loading waveform: haversine waveform. Via equation (9), $E_{3\text{-}2\text{-}1} = 16{,}872$ MPa.
$R_{3\text{-}2\text{-}1} = E_{3\text{-}2\text{-}1}/E_B < 1$. Via equation (***), wavelength: $D_{3\text{-}2\text{-}1} = 60.980$ cm, loading time:

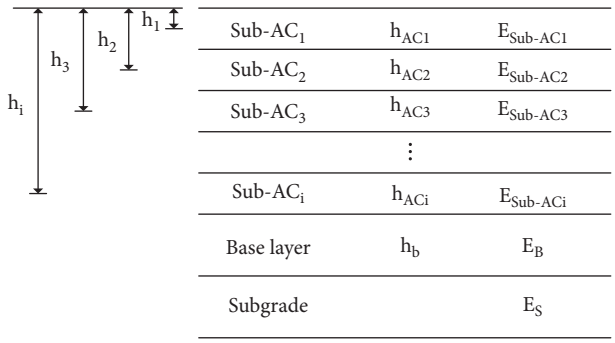

Figure 6: Typical pavement structure.

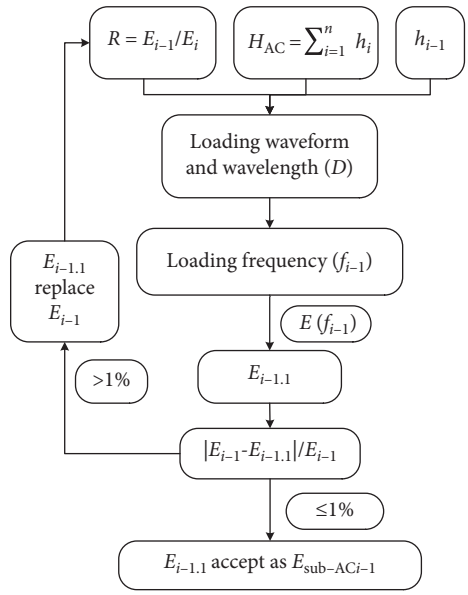

Figure 7: Dynamic modulus obtaining methodology flow chart.

$T_{3\text{-}2\text{-}1} = 0.0305$ s, and loading frequency: $f_{3\text{-}2\text{-}1} = 32.798$ Hz. Via equation (***), $E_{3\text{-}2\text{-}1\text{-}1} = 16{,}837$ MPa. Then, $|E_{3\text{-}2\text{-}1\text{-}1}\text{-}E_{3\text{-}2\text{-}1}|/E_{3\text{-}2\text{-}1} \le 1\%$; therefore, $E_3 = E_{3\text{-}2\text{-}1\text{-}1} = 16{,}837$ MPa.

Therefore, when the loading waveform was bell, $E_3 = 14{,}001$ MPa, wavelength: $D_3 = 60.138$ cm, and loading frequency: $f_3 = 33.257$ Hz.

When the loading waveform was haversine, $E_3 = 16{,}837$ MPa, wavelength: $D_3 = 60.980$ cm, and loading frequency: $f_3 = 32.798$ Hz.

(2) $h_2 = 7$ cm. The modulus at the a depth of 7 cm was assumed as $E_2 = 15{,}000$ MPa.

Haversine was the loading waveform at the depth of 7 cm.

(2.1) When $E_3 = 14{,}001$ MPa, $1 < R_{2\text{-}1} = E_2/E_3$. Via equation (***), wavelength: $D_{2\text{-}1} = 45.650$ cm, loading time: $T_{2\text{-}1} = 0.0228$ s, and loading frequency: $f_{2\text{-}1} = 43.812$ Hz, and via equation (10), $E_{2\text{-}1} = 15{,}864$ MPa.

$1 < R_{2\text{-}1\text{-}1} = E_{2\text{-}1}/E_3$. Via equation (***), wavelength: $D_{2\text{-}1\text{-}1} = 45.830$ cm, loading time: $T_{2\text{-}1\text{-}1} = 0.0229$ s, and loading frequency: $f_{2\text{-}1\text{-}1} = 43.639$ Hz, and via equation (10), $E_{2\text{-}1\text{-}1} = 15{,}855$ MPa. Then, $|E_{2\text{-}1\text{-}1}\text{-}E_{2\text{-}1}|/E_{2\text{-}b\text{-}1} \le 1\%$; therefore, $E_2 = E_{2\text{-}1\text{-}1} = 15{,}855$ MPa.

(2.2) When $E_3 = 16{,}837$ MPa, $R_{2\text{-}2} < 1$. Via equation (***), wavelength: $D_{2\text{-}2} = 45.121$ cm, loading time: $T_{2\text{-}2} = 0.0226$ s, and loading frequency: $f_{2\text{-}2} = 44.325$ Hz. Via equation (10), $E_{2\text{-}2} = 15{,}892$ MPa.

$R_{2\text{-}2\text{-}1} = E_{2\text{-}2}/E_3 < 1$. Via equation (***), wavelength: $D_{2\text{-}2\text{-}1} = 45.278$ cm, loading time: $T_{2\text{-}2\text{-}1} = 0.0226$ s, and loading frequency: $f_{2\text{-}2\text{-}1} = 44.172$ Hz, and via equation (10), $E_{2\text{-}2\text{-}1} = 15{,}884$ MPa. Then, $|E_{2\text{-}2\text{-}1}\text{-}E_{2\text{-}2}|/E_{2\text{-}2} \le 1\%$; therefore, $E_2 = E_{2\text{-}2\text{-}1} = 15{,}884$ MPa.

Therefore, when $E_3 = 14{,}001$ MPa, $E_2 = 15{,}855$ MPa, wavelength: $D_2 = 45.8306$ cm, and loading frequency: $f_2 = 43.639$ Hz;

Table 2: Pavement structure and loading waveform.

Pavement structure	Material	Thickness (cm)	Loading waveform
Top AC layer	AC-13 base asphalt (PG 64-22)	4	Square/haversine
Middle AC layer	AC-20 base asphalt (PG 64-22)	6	Haversine/bell
Bottom AC layer	AC-25 base asphalt (PG 64-22)	8	Haversine/bell
Base	Cement-stabilized crushed stone	15	N/A
Base	Cement-stabilized crushed stone	15	N/A
Subgrade	N/A	N/A	N/A

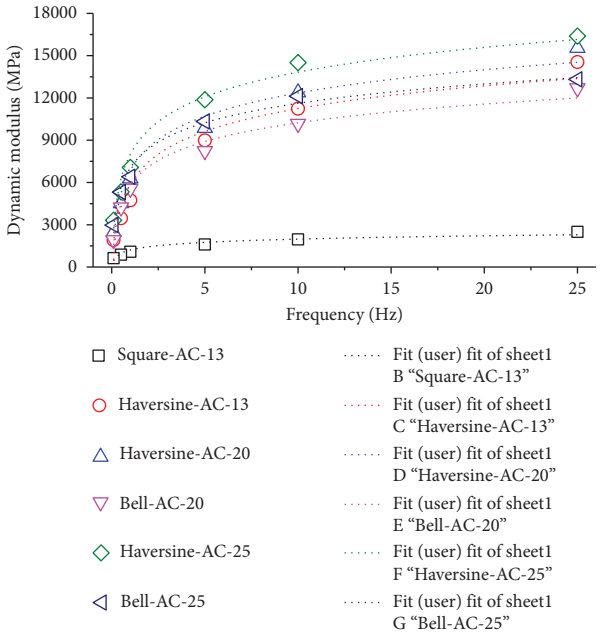

Figure 8: Dynamic modulus under different loading waveforms at 21°C.

When $E_3 = 16{,}837$ MPa, $E_2 = 15{,}884$ MPa, wavelength: $D_2 = 45.278$ cm, and loading frequency: $f_2 = 44.172$ Hz;

(3) $h_1 = 2$ cm.

$h_1 < 2.5$ cm, the square waveform was suitable, wavelength: $D_1 = 21.7$ cm, loading time: $T_1 = 0.00868$ s, and loading frequency: $f_1 = 92.166$ Hz, and via equation (14), $E_1 = 2{,}728$ MPa.

7. Conclusions

The 3D-FE model incorporating with the measured TPCP was utilized for calculating the vertical compressive stresses in AC layers. Based on extensive calculation and numerical fitting, proper loading waveforms and new wavelength calculation equations were proposed for the laboratory dynamic modulus test. The conclusions could be drawn as follows:

(1) Vertical compressive stress pulse is not always the same. The vertical compressive stress pulse tends to approach a square waveform when the position of interest is near the pavement surface. Then, it approaches to haversine with the increasing of depth. At greater pavement depths (i.e., 10 cm), the shape of the vertical compressive stress pulse changes to a bell waveform.

(2) The square waveform could be suitable merely with depths less than 2.5 cm; however, haversine and bell waveform could be more widely applicable. Additionally, haversine and bell waveforms could be suitable in some depth simultaneously.

(3) The waveform and wavelength vary at different positions beneath the pavement surface. The method to select a suitable waveform in the AC layer has been given. The equations to obtain loading wavelength within different loading waveforms at different depths are proposed.

(4) According to the method of recommendation of suitable waveforms and wavelength, R and depth are the two main factors that influence the waveform and wavelength in the AC layer.

(5) The process to calculate the accurate dynamic modulus at different depths for the field AC layer under different waveforms and loading time through the laboratory test is presented.

Data Availability

Previously reported (pictures or tables) data used to support this study are included within the article. These prior studies (and datasets) are cited at relevant places within the text as references [15].

Conflicts of Interest

The authors declare no conflicts of interest regarding the publication of this paper.

Acknowledgments

The authors wish to thank Dr. Yalong Pi from A&M University and Dr. Yao Zhang from Southeast University for their suggestions for this study. This study was funded by the National Nature Science Foundation of China (no. 51878168) and Open Research Fund of National Engineering Laboratory for Advanced Road Materials (no. NLARM-ORF-2018-01).

References

[1] NCHRP, "Guide for mechanistic-empirical design of new and rehabilitated pavement structures," Final Report 1-37A, NCHRP, Washington DC, USA, 2004.

[2] AASHTO TP 62-03, *Standard Method of Test for Determining Dynamic Modulus of Hot-Mix Asphalt Concrete Mixtures*, American Association of State Highway and Transportation Officials, Washington, DC, USA, 2005.

[3] H. E. I. Nur, D. Singh, and Z. P. E. Musharraf, "Dynamic modulus-based field rut prediction model from an instrumented pavement section," *Procedia-Social and Behavioral Sciences*, vol. 104, pp. 129–138, 2013.

[4] A. S. M. A. Rahman, M. R. Islam, and R. A. Tarefder, "Dynamic modulus and phase angle models for New Mexico's superpave mixtures," *Road Materials & Pavement Design*, vol. 20, no. 3, pp. 1–14, 2019.

[5] N. Su, F. Xiao, J. Wang et al., "Precision analysis of sigmoidal master curve model for dynamic modulus of asphalt mixtures," *Journal of Materials in Civil Engineering*, vol. 30, no. 11, article 04018290, 2018.

[6] Y. Ali, M. Irfan, S. Ahmed, S. Khanzada, and T. Mahmood, "Investigation of factors affecting dynamic modulus and phase angle of various asphalt concrete mixtures," *Materials and Structures*, vol. 49, no. 3, pp. 857–868, 2016.

[7] M. Irfan, A. S. Waraich, S. Ahmed et al., "Characterization of various plant-produced asphalt concrete mixtures using dynamic modulus test," *Advances in Materials Science and Engineering*, vol. 2016, Article ID 5618427, 12 pages, 2016.

[8] A. R. Ghanizadeh and M. Fakhri, "Effect of waveform, duration and rest period on the resilient modulus of asphalt mixes," *Procedia-Social and Behavioral Sciences*, vol. 104, no. 3, pp. 79–88, 2013.

[9] R. D. Barksdale, "Compressive stress pulse times in flexible pavements for use in dynamic testing," *Highway Research Record*, vol. 345, no. 4, 1971.

[10] X. Hu, F. Zhou, S. Hu, and L. F. Walubita, "Proposed loading waveforms and loading time equations for mechanistic-empirical pavement design and analysis," *Journal of Transportation Engineering*, vol. 136, no. 6, pp. 518–527, 2010.

[11] A. Loulizi, I. L. Al-Qadi, S. Lahouar, and T. E. Freeman, "Measurement of vertical compressive stress pulse in flexible pavements: representation for dynamic loading tests," *Transportation Research Record: Journal of Transportation Research Board*, vol. 1816, no. 1, pp. 125–136, 2002.

[12] S. F. Brown, "Determination of young's modulus for bituminous materials in pavement design," *Highway Research Record*, vol. 431, pp. 38–49, 1973.

[13] Y. H. Huang, *Pavement Analysis and Design*, Prentice Hall, Inc., Upper Saddle River, NJ, USA, 2nd edition, 2004.

[14] D.-W. Park, A. E. Martin, and E. Masad, "Effects of non-uniform tire contact stresses on pavement response," *Journal of Transportation Engineering*, vol. 131, no. 11, pp. 873–879, 2005.

[15] L. J. Sun, *Structure Behavior Study for Asphalt Pavements*, China Communications Press, Beijing, China, 2nd edition 2005, in Chinese.

[16] I. L. Al-Qadi and H. Wang, "Evaluation of pavement damage due to new tire designs," Report No. FHWA-ICT-09-048, Illinois Center for Transportation, Rantoul, IL, USA, 2009.

[17] L. A. Myers, R. Roque, and B. E. Ruth, "Mechanisms of surface-initiated longitudinal wheel path cracks in high-type bituminous pavements," *Journal of Association of Asphalt Paving Technologists*, vol. 67, pp. 401–432, 1998.

[18] A. Loulizi, I. L. Al-Qadi, and M. Elseifi, "Difference between in situ flexible pavement measured and calculated stresses and strains," *Journal of Transportation Engineering*, vol. 132, no. 7, pp. 574–579, 2006.

[19] H. Wang and I. L. Al-Qadi, "Combined effect of moving wheel loading and three-dimensional contact stresses on perpetual pavement responses," *Transportation Research Record: Journal of Transportation Research Board*, vol. 2095, no. 1, pp. 53–61, 2009.

[20] C. Zopf, I. Wollny, M. Kaliske, A. Zeißler, and F. Wellner, "Numerical modelling of tyre-pavement-interaction phenomena: constitutive description of asphalt behaviour based on triaxial material tests," *Road Materials and Pavement Design*, vol. 16, no. 1, pp. 133–153, 2014.

[21] X. Hu and L. F. Walubita, "Modelling tensile strain response in asphalt pavements," *Road Materials and Pavement Design*, vol. 10, no. 1, pp. 125–154, 2009.

[22] M. De Beer, C. Fisher, and F. J. Jooste, "Determination of pneumatic tyre/pavement interface contact stresses under moving loads and some effects on pavements with thin asphalt surfacing layers," in *Proceedings of the Eight International Conference on Asphalt Pavements*, vol. 1, pp. 179–227, Seattle, WA, USA, August 1997.

[23] R. V. Siddharthan, N. Krishnamenon, M. El-Mously, and P. E. Sebaaly, "Investigation of tire contact stress distributions on pavement response," *Journal of Transportation Engineering*, vol. 128, no. 2, pp. 136–144, 2002.

[24] L. Ann Myers, R. Roque, B. E. Ruth, and C. Drakos, "Measurement of contact stresses for different truck tire types to evaluate their influence on near-surface cracking and rutting," *Transportation Research Record: Journal of Transportation Research Board*, vol. 1655, no. 1, pp. 175–184, 1999.

[25] I. L. Al-Qadi and P. J. Yoo, "Effect of surface tangential contact stresses on flexible pavement response (with discussion)," *Journal of Association of Asphalt Paving Technologists*, vol. 76, pp. 663–692, 2007.

[26] JTG F40-2004, *Technical Specification for Construction of Highway Asphalt Pavements*, People Transportation Press, Beijing, China, 2004, in Chinese.

[27] JTG D50-2017, *Specifications for Design of Highway Asphalt Pavements*, People Transportation Press, Beijing, China, 2017, in Chinese.